

Titre: The correlation of austenite stability and sequence of strain accommodation during room temperature deformation of a duplex lightweight steel
Title:

Auteurs: Behnam Mirshekari, Abbas Zarei-Hanzaki, Aidin Barabi, Hamid Reza Abedi, Seung-Joon Lee, & Hidetoshi Fujii
Authors:

Date: 2021

Type: Article de revue / Article


Référence: Mirshekari, B., Zarei-Hanzaki, A., Barabi, A., Abedi, H. R., Lee, S.-J., & Fujii, H. (2021). The correlation of austenite stability and sequence of strain accommodation during room temperature deformation of a duplex lightweight steel. *Journal of Materials Research and Technology*, 13, 1923-1932.
Citation: <https://doi.org/10.1016/j.jmrt.2021.05.082>

 **Document en libre accès dans PolyPublie**
Open Access document in PolyPublie

URL de PolyPublie: <https://publications.polymtl.ca/48708/>
PolyPublie URL:

Version: Version officielle de l'éditeur / Published version
Révisé par les pairs / Refereed

Conditions d'utilisation: CC BY-NC-ND
Terms of Use:

 **Document publié chez l'éditeur officiel**
Document issued by the official publisher

Titre de la revue: Journal of Materials Research and Technology (vol. 13)
Journal Title:

Maison d'édition: Elsevier Editora Ltda
Publisher:

URL officiel: <https://doi.org/10.1016/j.jmrt.2021.05.082>
Official URL:

Mention légale: © 2021 Mirshekari, B., Zarei-Hanzaki, A., Barabi, A., Abedi, H. R., Lee, S.-J., & Fujii, H. Published by Elsevier B.V. This is an open access article under the CC BY-NC-ND license (<http://creativecommons.org/licenses/by-nc-nd/4.0/>).
Legal notice:

Available online at www.sciencedirect.com

jmr&t
Journal of Materials Research and Technology
journal homepage: www.elsevier.com/locate/jmrt



Original Article

The correlation of austenite stability and sequence of strain accommodation during room temperature deformation of a duplex lightweight steel



B. Mirshekari ^a, A. Zarei-Hanzaki ^{a,**}, A. Barabi ^{a,b}, H.R. Abedi ^{c,*},
S.-J. Lee ^d, H. Fujii ^e

^a Hot Deformation and Thermomechanical Processing Laboratory of High Performance Engineering Materials, School of Metallurgy and Materials Engineering, College of Engineering, University of Tehran, Tehran, Iran

^b Department of Mechanical Engineering, Polytechnique Montréal, Montréal, Québec, Canada

^c School of Metallurgy & Materials Engineering, Iran University of Science and Technology (IUTS), Tehran, Iran

^d Department of Advanced Materials Engineering, Korea Polytechnic University, Siheung-si, 15073, Republic of Korea

^e Joining and Welding Research Institute, Osaka University, 11-1, Mihogaoka, Ibaraki, Osaka, 567-0047, Japan

ARTICLE INFO

Article history:

Received 11 March 2021

Accepted 28 May 2021

Available online 6 June 2021

Keywords:

Strain accommodation sequences

Austenite stability

Work hardening rate

Transformation induced plasticity, (TRIP)

Hardening stages

ABSTRACT

The effect of austenite stability on the sequence of room temperature strain accommodation has been investigated in Fe-0.07C-11.15Mn-5.6Al-0.12Si lightweight steel through employing interrupted tensile tests coupled with electron backscattered diffraction analysis. It has been found that in the microstructure holding finest grain size, the strain is mainly accommodated through austenite via transformation induced plasticity (TRIP) effect during the first stage of deformation (up to the true strain of 0.03), which hinders Kernel Average Misorientation (KAM) increment in constituent phases. Although, high stability of austenite limits the first deformation stage to low strains and the contribution of ferrite along with austenite is traced in the following stages as indicated by KAM increment, leading to higher TRIPing saturation strains, due to this simultaneous strain accommodation. However, by lowering the austenite stability, strain accommodation behaves differently in which case, low stability of the austenite leads to intensified TRIP effect which accommodates the imposed strains to larger strains (up to the true strain of 0.08) during the first stage. Respectively, due to intense TRIPing during the mentioned stage, KAM of both constituent phases remains low, but this severe solo accommodation decreases the fraction of austenite dramatically and saturates the capability for TRIP effect. Subsequently, load transfers from austenite to the ferrite during the second deformation stage leading to a sharp reduction in work hardening and increment in KAM value. Despite the microstructure holding higher austenite stability which represents simultaneous accommodation, sequential strain accommodation deteriorates the hardening capability and the strength/ductility balance of the material.

© 2021 The Author(s). Published by Elsevier B.V. This is an open access article under the CC BY-NC-ND license (<http://creativecommons.org/licenses/by-nc-nd/4.0/>).

* Corresponding author.

** Corresponding author.

E-mail addresses: zareih@ut.ac.ir (A. Zarei-Hanzaki), habedi@iust.ac.ir (H.R. Abedi).<https://doi.org/10.1016/j.jmrt.2021.05.082>2238-7854/© 2021 The Author(s). Published by Elsevier B.V. This is an open access article under the CC BY-NC-ND license (<http://creativecommons.org/licenses/by-nc-nd/4.0/>).

1. Introduction

Duplex lightweight steels have shown a good combination of strength and ductility owing to the co-existence of both ferrite and austenite phases. This remarkable mechanical property is related to deformation behavior of constituent phases [1–3]. Ferrite accommodates the imposed strain by dislocation slip via numerous slip systems [4–6]. On the other hand, austenite contributes to strain accommodation by distinctive mechanisms such as dislocation slip, twinning induced plasticity (TWIP) and transformation induced plasticity (TRIP) [7–9]. It has been observed that in particular, transformation from soft metastable austenite phase into hard martensite phase upon activation by mechanical stimulus so called TRIPing, increases the work hardening rate and delays necking resulting in an increment of elongation along with strength [10–12].

This presence of multi-phases with different deformation behaviors and mechanical properties such as ferrite and austenite is the basis of strain partitioning and sequential deformation of phases which effectively alters the mechanical properties [13–16]. During deformation, the softer phase yields first and after sufficient work hardening, stress is transferred on the harder phases to cause them to yield. He et al. [17] have conducted nano-indentation on a medium Mn steel with 30% austenite fraction and reported that ferrite is mainly responsible for the initiation of macroscopic yielding. Seo et al. [18] have also conducted nano-indentation on a cold rolled and annealed lightweight steel determining the deformation behavior of constituent phases. It was stated that ferrite is the softer phase and responsible for yielding and austenite contributes secondly during further deformation. On the other hand, Imandoust et al. [19] reported a brittle behavior for ferrite owing to the existence of nanometric ordered phases. On the other hand, Melero et al. [20] concluded from an in-situ synchrotron study on a duplex TRIP steel that the evolution of load partitioning takes place before reaching macroscopic yielding and the macroscopic yielding is mainly governed by austenite. The strain partitioning in austenite as the softer phase is a controversial issue that is basically related to the alloying compositions and alloy processing routes. This inconsistency of load partitioning becomes even more complex after yielding due to progressive yielding of different grains in a polycrystalline material. Many researchers declared that by optimizing the strain partitioning, mechanical properties can be improved as well. Li et al. [6] have reported that γ (face centered cubic) \rightarrow ϵ (hexagonal close packed) \rightarrow α' (body centered cubic) transformation sequence demonstrated a compatible strain evolution in austenite and ferrite leading to a good combination of strength and ductility while direct $\gamma \rightarrow \alpha'$ resulted in a strain localization from austenite to ferrite and deterioration of mechanical properties. Herrera et al. [21] aimed at an alloying strategy to acquire optimum austenite stability for continuous TRIPing achievement during deformation, which resulted in superior mechanical properties. More to this, in our previous work it was observed that by austenite stability optimization, the work hardening behavior was significantly improved

while poor austenite stability deteriorated it [22,23]. It is believed that the state of austenite stability directly impacts the strain partitioning and subsequent substructure developments of the material but such idea was not investigated in details in previous works.

By consideration of mentioned researches in literature, the study of phase accommodation sequence in lightweight steels is worthy of investigation. To the best of the authors' knowledge, the aim of the present research is to investigate the effective role of austenite stability and constituent phases on strain accommodation sequences from the onset of yielding up to fracture and their effect on mechanical properties. In this regard, the changes in texture and kernel average misorientation (KAM) in the course of room temperature deformation are tracked by interruption tests. In order to determine the optimum strain accommodation sequence, different microstructures were fabricated utilizing friction stir processing.

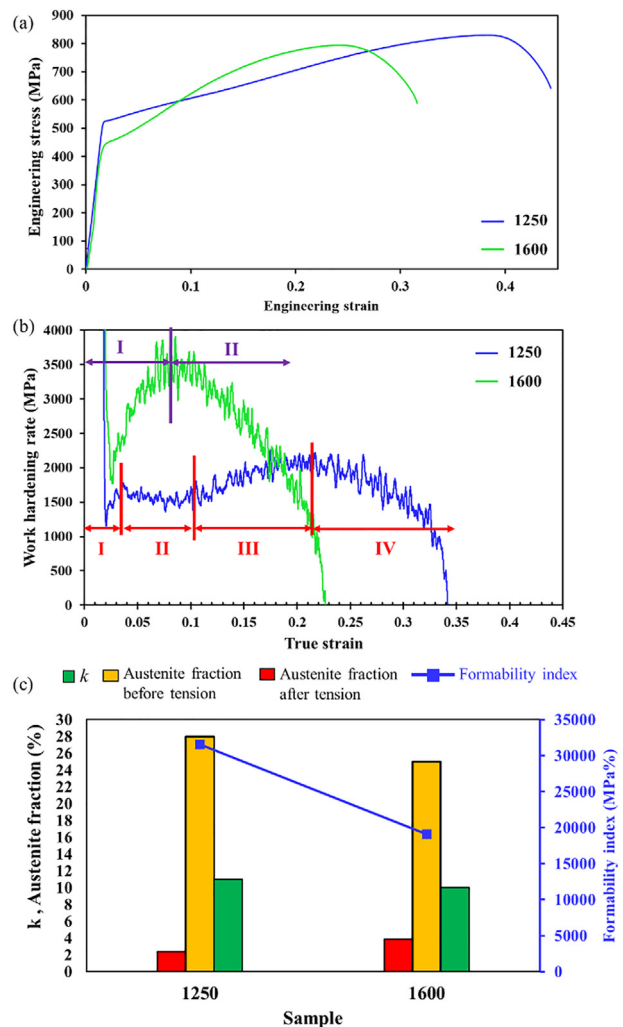


Fig. 1 – (a) Engineering Stress–Strain, (b) Work hardening rate–strain curve and (c) Stability coefficient, fraction of austenite prior and subsequent to tension along with formability index of FSPed samples.

2. Experimental

2.1. Material and process

The fabrication method of utilized material with the chemical composition of Fe-0.07C-11.15Mn-5.6Al-0.12Si (wt.%) has been reported in [22]. The hot rolled plates were cut into $6 \times 30 \times 100$ mm rectangular specimens, and subjected to annealing at 950 °C under argon atmosphere. Respectively, after annealing, plates were subjected to FSP under the rotational speeds of 1250 rpm and 1600 rpm and with constant traverse speed of 40 mm min⁻¹. All samples were quenched after annealing or FSP and subjected to tensile test with strain rate of be 3×10^{-3} s⁻¹ by SANTAM-STM50 universal testing machine. Tensile test samples were extracted from the middle of the stir zone parallel to process direction. Microstructural characterizations were investigated by means of optical microscopy (OM) and electron back scattered diffraction (EBSD) and to do so, work pieces were sectioned in the transverse direction by EDM. The specimens were etched by 10% Nital solution for OM images and electro-polished in 90%CH₃COOH+10%HClO₄ at 15 V for 20s for EBSD analysis. A step size of 0.12 μm was selected for EBSD analysis. The acquired data was interpreted by orientation imaging microscopy software (OIM, TexSEM Laboratory).

3. Results and discussion

3.1. Mechanical properties

Fig.1 represents the mechanical properties and work hardening behavior of friction stir processed samples in which, by utilizing different rotational speeds of 1250 rpm and 1600 rpm (which will be referred to as 1250 sample and 1600 sample in the following), different mechanical response was observed as are reported in Table 1. To explain more, the highest UTS and elongation corresponds to 1250 sample combined with multi-stage hardening from the onset of yielding up to 0.03 strain (*stage*₁₂₅₀^I), a plateau-like behavior from 0.03 up to 0.10 strain (*stage*₁₂₅₀^{II}), a broad increment in work hardening up to 0.21 strain (*stage*₁₂₅₀^{III}) followed by a slow descending trend of work hardening up to fracture (*stage*₁₂₅₀^{IV}). However, 1600 sample illustrates a two-stage work hardening behavior comprising of a rapid hardening up to 0.08 strain in the first stage (*stage*₁₆₀₀^I) followed by a gradual decrement of work hardening up to fracture (*stage*₁₆₀₀^{II}) Fig. 1b.

As reported in our previous work [22], the origin of work hardening peaks was mainly attributed to the occurrence of TRIPing during tension, however, different stabilities, lead to

different behaviors. In this respect, 1250 sample showed superior mechanical properties due to lower stability in comparison with 1600 sample. This can be seen in the mechanical stability coefficient (*k*) of austenite in each sample in Fig. 1c. The expression of *k* is as follow [24]:

$$k = \frac{\ln(V_{\gamma 0}) - \ln(V_{\gamma e})}{\epsilon} \tag{1}$$

where *V*_{γ0} and *V*_{γe} denote the volume fraction of austenite prior and subsequent to deformation up to the true strain of ϵ and both fractions were calculated through X-ray analysis. The results indicate that the superiority of mechanical properties is scaled inversely with *k* and therefore, is directly related to the stability of austenite whilst, decrement in austenite fraction indicate of formation of TRIPing during tension.

Having all said, in order to fully understand the role of austenite stability during these multi-stage work hardening rate, interrupted tensile tests have been applied at the end of *stage*₁₂₅₀^I, *stage*₁₂₅₀^{III} and *stage*₁₆₀₀^{II} (which will be referred to as *Interruption I*, *Interruption II* and *Interruption III* in the following) and are discussed in the following.

3.2. Microstructural evolution in 1250 sample during tension

The phase map and KAM of as-processed, *Interruption I*, *Interruption II* and fracture of 1250 sample along with austenite grain size distribution of as-processed 1250 sample have been illustrated Fig. 2 along with the average KAM value of ferrite and austenite. Phase maps can demonstrate the deformation induced transformation of austenite during tension while KAM maps serve as a measure of deformation-induced local orientation gradients [21]. The as-processed microstructure of 1250 sample has been investigated in details in our previous work but in general, it can be said that the structure is comprised of both BCC (ferrite and thermal martensite) and FCC (austenite) structures with the grain size of 1.5 μm and 3 μm for ferrite and austenite, respectively along with a low fraction of LAGBs and KAM in ferrite and austenite (Fig. 2 a) [22]. By imposing strain up to the end of *stage*₁₂₅₀^I, a slight decrease in KAM of austenite can be observed despite the KAM of ferrite which remains almost constant. These changes in KAM of constituent phases are in contrast with other reports in which researchers reported a mild increment in KAM [6,25,26]. However, further straining up to the end of *stage*₁₂₅₀^{III} leads to increment of KAM in both austenite and ferrite and this trend continues up to fracture which results in high KAM value of both austenite and ferrite (Fig. 5 d) similar to mentioned reports. This is accompanied by a persistent increase in LAGB in each stage of deformation as can be observed through Fig. 2 a to d.

In order to better understand the behavior of each accommodative phase during tension, the inverse pole figure (IPF) of ferrite and austenite in as processed, interrupted and fractured samples of 1250 samples are depicted in Fig. 3. Since no further strain can be accommodated by martensite after complete austenite to martensite transformation, IPF of thermal and deformation martensite has been removed in order to directly investigate the texture evolution of both

Table 1 – Mechanical properties and formability index (UTS × Elongation) of 1250 sample and 1600 sample.

Sample	Yield Stress (MPa)	UTS (MPa)	Elongation (%)	Formability Index (MPa%)
1250 rpm	524	830	38	31,540
1600 rpm	422	794	24	19,056

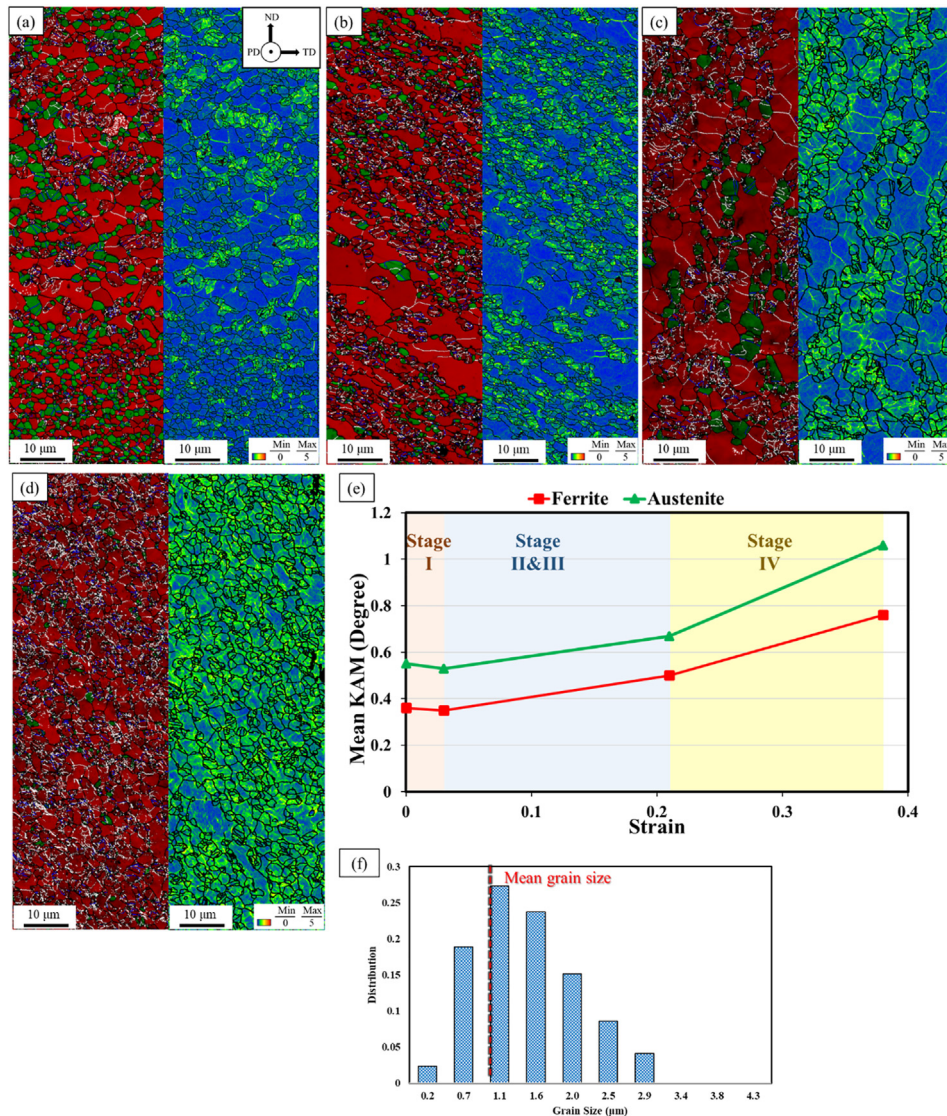


Fig. 2 – Phase map and kernel average misorientation of (a) 1250 sample in as-processed condition, (b) Interruption I, (c) Interruption II, (d) fractured sample, (e) mean KAM value for both austenite and ferrite in each stage and (f) grain size distribution of austenite (White and black lines represent low and high angle grain boundaries, respectively).

accommodative phases. In this respect, Austenite shows a strong $\langle 001 \rangle // \text{TA}$ (Tensile Axis) component which is attributed to deformed austenite grains and a weak $\langle 111 \rangle // \text{TA}$ component which is attributed to recrystallized ones while ferrite shows a strong $\langle 101 \rangle$ component, prior to tension (Fig. 3 a&b) [3,27]. At the first stage of deformation (stage_{1250}^I), $\langle 001 \rangle // \text{TA}$ component in austenite vanishes completely and inclines toward $\langle 111 \rangle$ component while texture of ferrite deviates partially from $\langle 101 \rangle // \text{TA}$ to $\langle 001 \rangle // \text{TA}$ still showing strong $\langle 101 \rangle // \text{TA}$ component (Fig. 3 c&d). Noticeably, the $\langle 101 \rangle // \text{Ta}$ component in ferrite is reported to be its susceptible orientation for deformation accommodation and deviation from it during tension is an unexpected behavior. Moreover, it should be noted that such sharp alterations in grain orientations takes place with a small amount of imposed strains (0.03).

Since the texture of ferrite has deviated from its susceptible orientation during stage_{1250}^I along with a constant value of its KAM it can be concluded that ferrite played a neutral role during this stage while from sharp alternations in austenitic orientation and KAM it can be concluded that austenite is the main accommodating phase during this stage. This solo accommodation of austenite imposes stress to ferrite due to phase compatibility of the structure, forming a high density of GNDs at austenite/ferrite or martensite/ferrite interface and deviates the ferrite from its susceptible orientation of deformation as observed in (Fig. 2 b) [6]. More to this, there are two main reasons for formation of $\langle 111 \rangle // \text{TA}$ component in austenite. Firstly, it has been reported that $\langle 001 \rangle // \text{TA}$ austenite grains transform to martensite during tension, preferentially [3,20,28]. Hence, the annihilation of $\langle 001 \rangle // \text{TA}$ austenite grains stemming from martensitic transformation

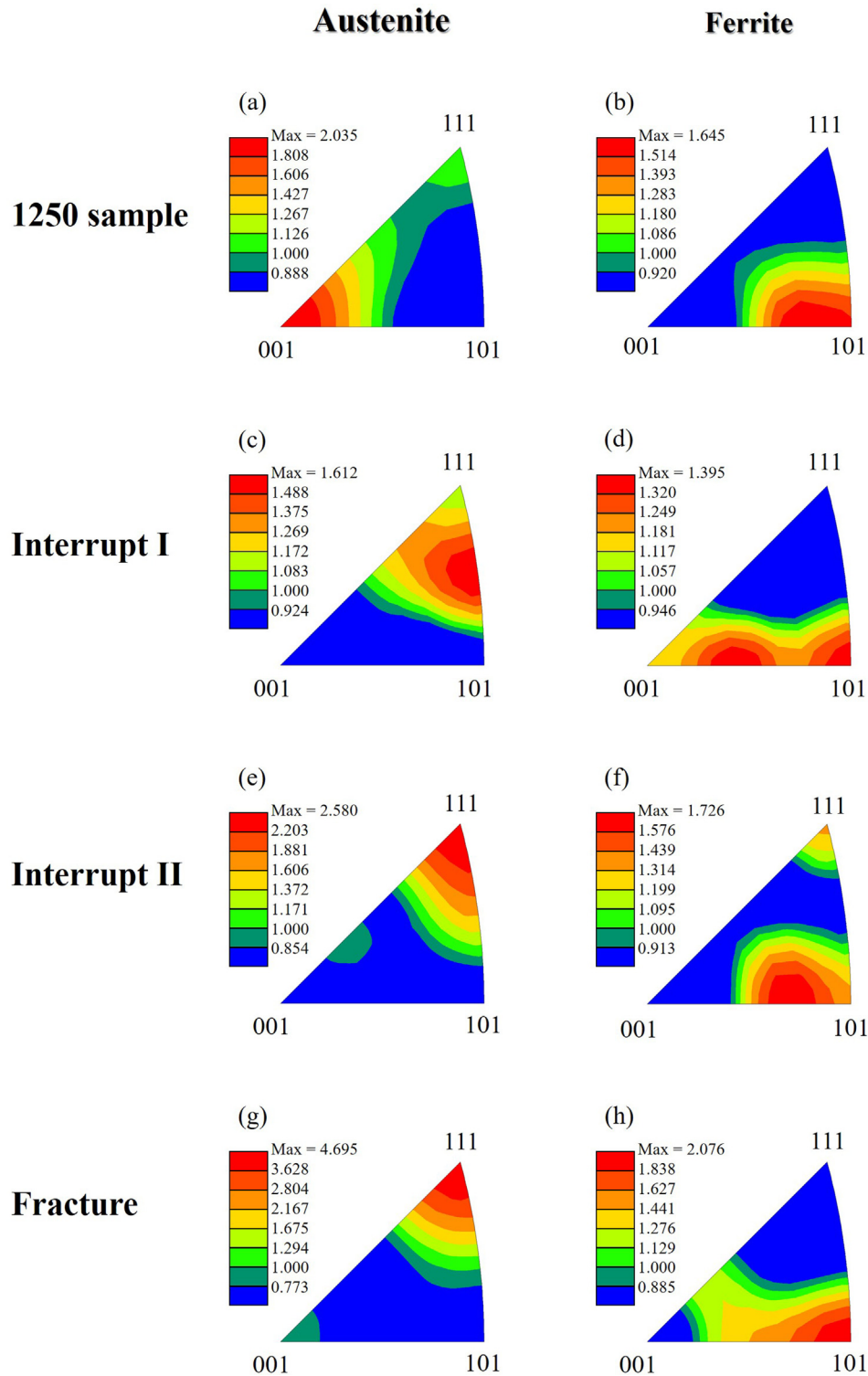


Fig. 3 – Texture evolution of both ferrite and austenite in the 1250 sample, *Interrupt I*, *Interrupt II* and fractured sample expressed in terms of the inverse pole figures.

gives rise to $\langle 111 \rangle // TA$ component in austenite. Secondly, unfavorable austenite grains for transformation, accommodate the deformation by dislocation accumulation which, then again, is associated with rotation of austenite toward

$\langle 111 \rangle // TA$. Therefore, it can be concluded that extension of work hardening rate increment in $stage_{1250}^I$ is directly related to occurrence of TRIPing and hence is affected by the stability of austenite. Based on what has been asserted, although a

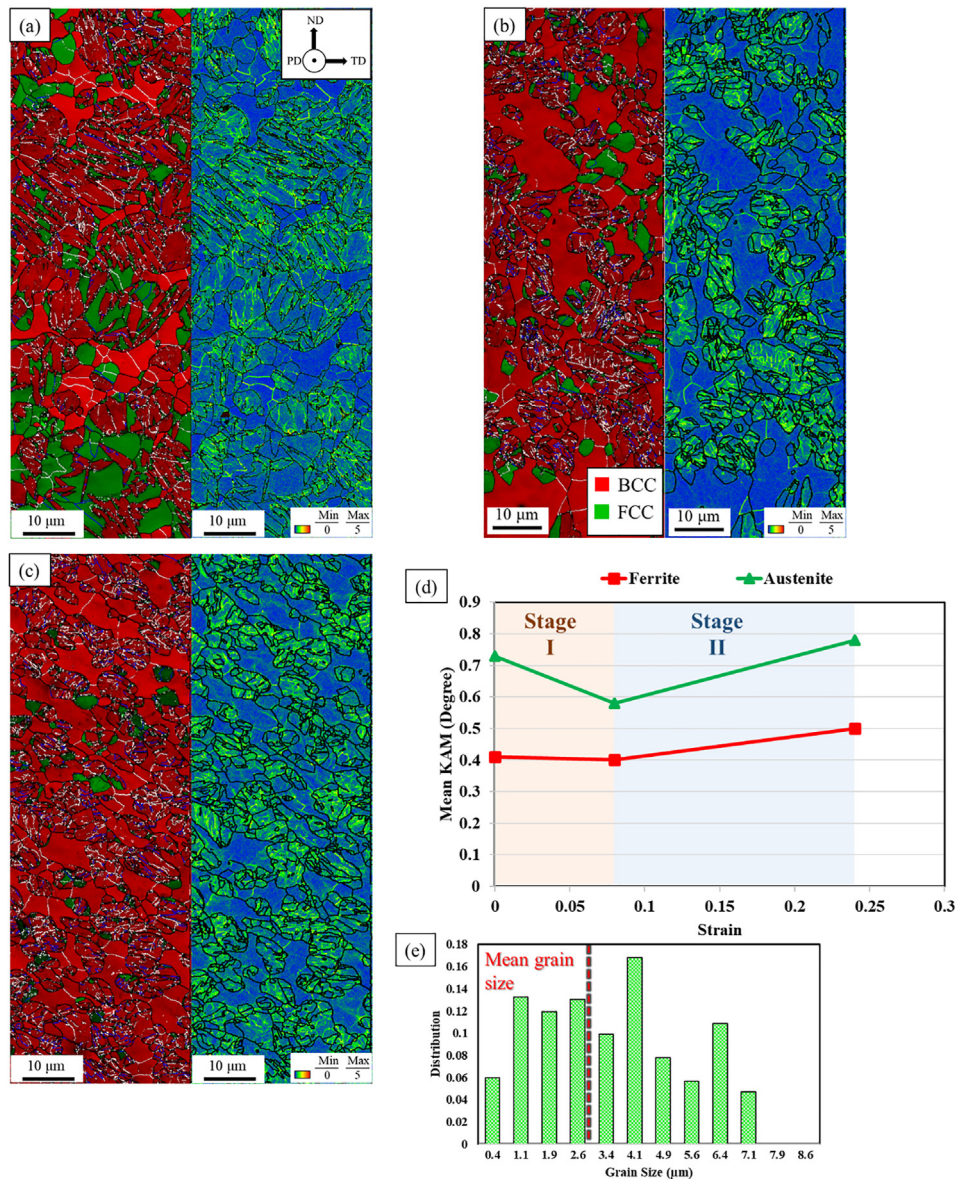


Fig. 4 – Phase map and kernel average misorientation of (a) 1600 sample in as-processed condition, (b) Interruption III, (c) fractured sample, (d) mean KAM value for both austenite and ferrite in each stage and (e) grain size distribution of austenite (White and black lines represent low and high angle grain boundaries, respectively).

large fraction of austenite grains are oriented along with preferred transformation orientation ($\langle 001 \rangle // TA$), but grain size distribution of austenite grains is not certified for a massive martensitic transformation due to small mean grain sizes (Fig. 2 f). Low fraction of suitable grains for the occurrence of TRIPing and low capability of dislocation accumulation in austenite limit the individual strain accommodation of austenite to small strains of 0.03 and the role of ferrite becomes effective at the beginning of $stage_{1250}^I$ along with austenite where simultaneous occurrence of TRIPing in austenite and dislocation accumulation in ferrite ends in a plateau-like in work hardening curve during [6].

As deformation continues, once the applied stress has overcome the critical stress for the transformation of less-

favorably oriented grains, the transformation intensifies and subsequently, gives rise to the work hardening rate and this is the beginning of $stage_{1250}^{III}$ during which, untransformed austenite grains and ferrite continue to rotate toward $\langle 111 \rangle // TA$ and $\langle 101 \rangle // TA$ as it can be seen in Fig. 3 e&f. Thus, at the end of $stage_{1250}^{III}$, both phases are aligned toward their susceptible rotation orientation. This is accompanied by increment in KAM value and LAGBs in both phases since dislocation accumulation is also taking place along with TRIPing (Fig. 2 e).

By further straining, since the fraction of retained austenite decreases and grains tends to rotate toward the orientation of $\langle 111 \rangle // TA$ (which is unsusceptible for TRIPing), thus the capability for TRIPing decreases during each stage [24,29]. Subsequently, during $stage_{1250}^{IV}$, role of austenite in strain

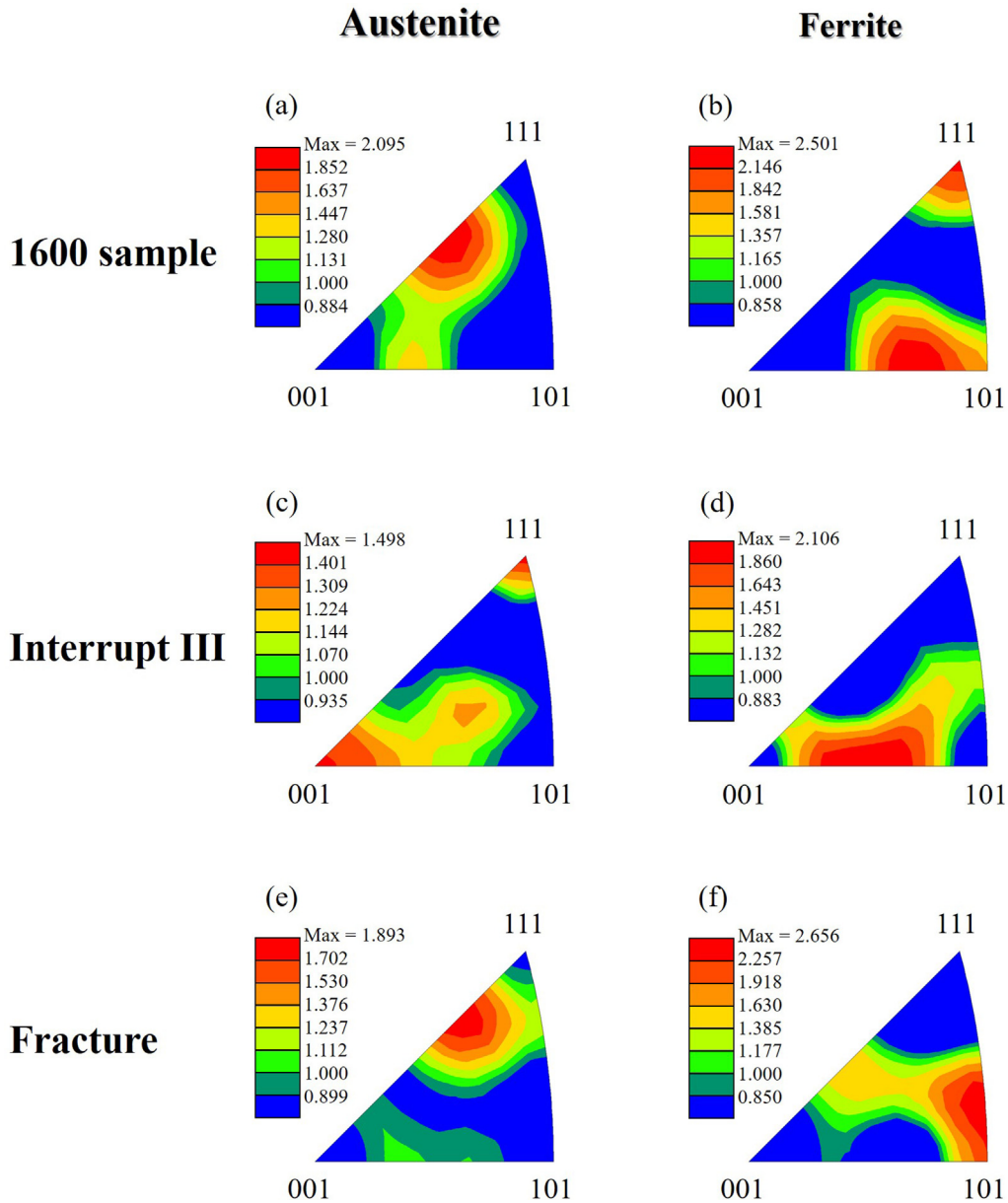


Fig. 5 – Texture evolution of both ferrite and austenite phases in the 1600 sample, Interruption III and fractured sample expressed in terms of the inverse pole figures.

accommodation starts to fade while the role ferrite becomes more dominant. Although, such shift in accommodation is being occurred gradually and continues until final fracture as it can be seen in the work hardening rate where the decreasing work hardening trend of ferrite, slowly overcomes the increasing work hardening trend of austenite which is due to the vast stability of austenite (Fig. 1 b). More to this, since both phases participate in strain accommodation until final fracture, KAM value and LAGBs in both phases increase continuously (Fig. 2 d&e) and their final orientation is aligned toward their susceptible rotation orientation (Fig. 3 g&h).

3.3. Microstructural evolution in 1600 sample during tension

Similarly, the phase map and KAM of as-processed, Interruption III, and fracture of 1600 sample along with the austenite grain size distribution of as-processed 1600 sample have been illustrated Fig. 4 along with the average KAM value of austenite and ferrite in each sample. Noteworthy, the detailed analysis of the as-processed microstructure of 1600 sample is reported elsewhere but in summary, it is comprised of ferrite with a mean grain size of 4 μm, austenite with mean grain size

of 3 μm (which are coarser than 1250) and thermal martensite. High KAM can be observed only in LAGBs in ferrite while austenite contains a high value of KAM stemmed from the compression stress of martensitic transformation [22]. Unlike 1250 *sample*, by imposing strain at the end of stage_{1600}^I , KAM of austenite decreases however, KAM of ferrite yet remains constant and is associated with neglectable changes in LAGBs fractions even though, 0.08 strain was applied (Fig. 4 b). These observed behaviors in the KAM value are related to sequential phase accommodation and strain partitioning same as 1250 *sample* but noticeably, strain partitioning is being intensified in 1600 *sample* since these behaviors continued until higher strains. By further straining during the stage_{1600}^{II} the KAM of both accommodative phases increases up to fracture along with fraction of LAGBs (Fig. 4 c & d).

Along with microstructural evolutions, the IPF of accommodative phases in 1600 *sample* has been demonstrated in Fig. 5. As-processed 1600 *sample* holds a different processed texture than 1250 *sample* as is represented in Fig. 5 a&b due to different utilized rotational speed. During stage_{1600}^I , a significant change in austenite texture is observed which is comprised of two strong $\langle 001 \rangle // \text{TA}$ and $\langle 111 \rangle // \text{TA}$ components (Fig. 5 c). Formation of multi-components during deformation conflicts with other reports and has not been reported before [3,5] and more to that, it is unlike austenite behavior in 1250 *sample*. On the other hand, orientation of ferrite is similar to observed behavior in 1250 *sample* where it deviates from its initial texture toward $\langle 001 \rangle // \text{TA}$ component (Fig. 5 d) but mentioned deviation is greater than the one observed in *Interruption I* which supports the anticipation that strain partitioning is greater in 1600 *sample*.

Based on pervious observations, since ferrite behaves similar to 1250 *sample* (KAM of ferrite remains low and ferrite deviates from its susceptible orientation with applying strain), it is reasonable to assume that similar to 1250 *sample*, ferrite role in strain accommodation during stage_{1600}^I must be neglected. However (i) more expanded hardening (ii) different behaviors in austenite rotation and (iii) KAM trend and in 1600 *sample* during the first stage with respect to 1250 *sample* must be stemmed from the lower austenite stability in 1600 *sample*.

In order to justify these dissimilarities, it should be mentioned that despite the fact that the as-processed texture of austenite is not orientated along with favorable orientation for transformation (Fig. 5 a), but martensitic transformation is more influenced by grain size rather than grain orientation [30]. Accordingly, based on Fig. 4 e, a high fraction of coarse grains in 1600 *sample* provides a suitable condition for transformation despite the unfavorable texture which expands the first stage to strains of 0.08 which is higher in comparison with 1250 *sample*. More to that, this intense TRIPing weakens the other accommodative mechanisms such as dislocation accumulation and subsequent rotation of austenite grains. Therefore, in the absence of grain rotation, compressed austenite gains become relaxed which decreases the KAM of austenite. Based on this, the observed austenite orientation in Fig. 5 c is mainly the texture of untransformed and un-rotated austenite grains.

During stage_{1600}^{II} the final orientation of ferrite is aligned with $\langle 101 \rangle // \text{TA}$ while austenite is partly deviated from

$\langle 111 \rangle // \text{TA}$ which is then again, an infrequent behavior since increment in KAM value of both phases, dictates that both accommodated strain. In order to justify these results, it should be noted that individual accommodation of strain by austenite along with a high potential for martensitic transformation in coarse austenite grains results in a rapid annihilation of austenite fraction and early saturation of TRIP effect during the first stage. Therefore, during stage_{1600}^{II} , ferrite accommodates most of the strain while austenite accommodation either with transformation or rotation becomes less significant. This is observable in KAM increment of both ferrite and austenite but with a sharp descending trend in work hardening rate which confirms the mentioned explanation. More on that, during the second stage, since ferrite accommodates most of the strain, severe rotation of ferrite grains imposes a strain to untransformed austenite grains and deviate austenite from its susceptible rotation orientation ($\langle 111 \rangle // \text{TA}$) which indicates that austenite played a neutral role at the end of straining while ferrite grains are aligned toward the susceptible $\langle 101 \rangle // \text{TA}$ orientation, indicating that ferrite participated in strain accommodation until final fracture.

4. Conclusion

In the present work, the microstructural evolutions during tensile tests of two friction stir processed lightweight steels with various austenite stabilities were investigated and the following results were obtained:

- During stage_{1250}^I , the imposed strain was mainly accommodated via TRIPing in small portioned austenite grains which held lower stability in comparison to other grains. This hindered the increment in KAM and depletion of $\langle 001 \rangle // \text{TA}$ component and gave intensity to $\langle 111 \rangle // \text{TA}$ component. This is while since ferrite played a neutral role its KAM remained constant and solo accommodation of austenite imposed stresses to ferrite which deviated it from its susceptible deformation orientation ($\langle 101 \rangle // \text{TA}$).
- Due to the high stability of austenite grains and low capability for grain rotations in 1250 *sample*, ferrite effective participation in strain accommodation commenced from the onset of stage_{1250}^{II} along with the participation of more stable austenite grains by both TRIPing and grain rotation in austenite and dislocation accumulation in ferrite leading to enhancement of work hardening rate up to the end of $\text{stage}_{1250}^{III}$, increment in KAM of both phases and observation of susceptible rotation orientation in each constituent phase subsequent to fracture.
- Due in part to the low average stability of austenite grains in 1600 *sample*, intense TRIPing dominated dislocation accumulation in both austenite and ferrite were which resulted in significant rapid work hardening and expansion of stage_{1600}^I up. This severe TRIPing hindered the increment of KAM of both phases to comprehensively high true strain (0.08). Moreover, intense TRIPing also led to early saturation and load transition from austenite to ferrite during

stage^{II}₁₆₀₀ which decreased the work hardening rate in this stage dramatically.

- Simultaneous accommodation of strain and consumption of the austenite for martensitic transformation in a wide strain range in 1250 sample was stemmed from high stability of austenite and it enhanced mechanical properties significantly, while sequential accommodation of strain and early saturation of TRIPing in 1600 sample took place due to low stability of austenite and deteriorates the mechanical properties.

Data availability

The raw/processed data required to reproduce these findings cannot be shared at this time as the data also forms part of an ongoing study.

Declaration of Competing Interest

The authors declare that they have no known competing financial interests or personal relationships that could have appeared to influence the work reported in this paper.

REFERENCES

- [1] Cho HH, Han HN, Hong ST, Park JH, Kwon YJ, Kim SH, et al. Microstructural analysis of friction stir welded ferritic stainless steel. *Mater Sci Eng, A* 2011;528:2889–94. <https://doi.org/10.1016/j.msea.2010.12.061>.
- [2] Chen S, Rana R, Haldar A, Ray RK. Current state of Fe-Mn-Al-C low density steels. *Prog Mater Sci* 2017;89:345–91. <https://doi.org/10.1016/j.pmatsci.2017.05.002>.
- [3] Blondé R, Jimenez-Melero E, Zhao L, Wright JP, Brück E, Van Der Zwaag S, et al. High-energy X-ray diffraction study on the temperature-dependent mechanical stability of retained austenite in low-alloyed TRIP steels. *Acta Mater* 2012;60:565–77. <https://doi.org/10.1016/j.actamat.2011.10.019>.
- [4] Kalantari AR, Zarei-Hanzaki A, Abedi HR, Hassanpour-Esfahani M, Park SJ, Park JY. Microstructure evolution and room temperature mechanical properties of a thermomechanically processed ferrite-based low density steel. *Mater Sci Eng, A* 2019;754:57–67. <https://doi.org/10.1016/j.msea.2019.03.048>.
- [5] Haghdadadi N, Cizek P, Beladi H, Hodgson PD. A novel high-strain-rate ferrite dynamic softening mechanism facilitated by the interphase in the austenite/ferrite microstructure. *Acta Mater* 2017;126:44–57. <https://doi.org/10.1016/j.actamat.2016.12.045>.
- [6] Li Y, Li W, Hu JC, Song HM, Jin XJ. Compatible strain evolution in two phases due to epsilon martensite transformation in duplex TRIP-assisted stainless steels with high hydrogen embrittlement resistance. *Int J Plast* 2017;88:53–69. <https://doi.org/10.1016/j.ijplas.2016.09.012>.
- [7] Sohn SS, Choi K, Kwak JH, Kim NJ, Lee S. Novel ferrite-austenite duplex lightweight steel with 77% ductility by transformation induced plasticity and twinning induced plasticity mechanisms. *Acta Mater* 2014;78:181–9. <https://doi.org/10.1016/j.actamat.2014.06.059>.
- [8] Abedi HR, Hanzaki AZ, Haghdadadi N, Hodgson PD. Substructure induced twinning in low density steel. *Scripta Mater* 2017;128:69–73. <https://doi.org/10.1016/j.scriptamat.2016.10.001>.
- [9] Barabi A, Zarei-Hanzaki A, Abedi H, Anoushe A, Cho JH. The correlation of macrostructure, microstructure, and texture with room temperature mechanical properties of a twinning-induced plasticity automotive steel after friction stir spot welding/processing. *Steel Res Int* 2018;89. <https://doi.org/10.1002/srin.201800245>.
- [10] Li ZC, Ding H, Misra RDK, Cai ZH. Microstructure-mechanical property relationship and austenite stability in medium-Mn TRIP steels: the effect of austenite-reverted transformation and quenching-tempering treatments. *Mater Sci Eng, A* 2017;682:211–9. <https://doi.org/10.1016/j.msea.2016.11.048>.
- [11] Kwon EP, Fujieda S, Shinoda K, Suzuki S. Characterization of transformed and deformed microstructures in transformation induced plasticity steels using electron backscattering diffraction. *Mater Sci Eng, A* 2011;528:5007–17. <https://doi.org/10.1016/j.msea.2011.03.033>.
- [12] Moshiri A, Zarei-Hanzaki A, Anoushe AS, Abedi HR, Mirshekari B, Berto F. Stress-relaxation viewpoint to study the room-temperature cyclic deformation behavior of a low-density steel. *Int J Fatig* 2020:105673. <https://doi.org/10.1016/j.ijfatigue.2020.105673>.
- [13] Sun B, Fazeli F, Scott C, Yan X, Liu Z, Qin X, et al. Critical role of strain partitioning and deformation twinning on cracking phenomenon occurring during cold rolling of two duplex medium manganese steels. *Scripta Mater* 2017;130:49–53. <https://doi.org/10.1016/j.scriptamat.2016.11.009>.
- [14] Das A, Tarafder S, Sivaprasad S, Chakrabarti D. Influence of microstructure and strain rate on the strain partitioning behaviour of dual phase steels. *Mater Sci Eng, A* 2019;754:348–60. <https://doi.org/10.1016/j.msea.2019.03.084>.
- [15] Asoushe MH, Hanzaki AZ, Abedi HR, Mirshekari B, Wegener T, Sajadifar SV, et al. Thermal stability, microstructure and texture evolution of thermomechanical processed AlCoCrFeNi_{2.1} eutectic high entropy alloy. *Mater Sci Eng, A* 2021;799:140012. <https://doi.org/10.1016/j.msea.2020.140012>.
- [16] Wang XG, Liu CH, He BB, Jiang C, Huang MX. Microscopic strain partitioning in Lüders band of an ultrafine-grained medium Mn steel. *Mater Sci Eng, A* 2019;761. <https://doi.org/10.1016/j.msea.2019.138050>.
- [17] He BB, Liang ZY, Huang MX. Nanoindentation investigation on the initiation of yield point phenomenon in a medium Mn steel. *Scripta Mater* 2018;150:134–8. <https://doi.org/10.1016/j.scriptamat.2018.03.015>.
- [18] Seo CH, Kwon KH, Choi K, Kim KH, Kwak JH, Lee S, et al. Deformation behavior of ferrite-austenite duplex lightweight Fe-Mn-Al-C steel. *Scripta Mater* 2012;66:519–22. <https://doi.org/10.1016/j.scriptamat.2011.12.026>.
- [19] Imandoust A, Zarei-Hanzaki A, Heshmati-Manesh S, Moemeni S, Changizian P. Effects of ferrite volume fraction on the tensile deformation characteristics of dual phase twinning induced plasticity steel. *Mater Des* 2014;53:99–105. <https://doi.org/10.1016/j.matdes.2013.06.033>.
- [20] Jimenez-Melero E, van Dijk NH, Zhao L, Sietsma J, Wright JP, van der Zwaag S. In situ synchrotron study on the interplay between martensite formation, texture evolution and load partitioning in low-alloyed TRIP steels. *Mater Sci Eng, A* 2011;528:6407–16. <https://doi.org/10.1016/j.msea.2011.04.087>.
- [21] Herrera C, Ponge D, Raabe D. Design of a novel Mn-based 1 GPa duplex stainless TRIP steel with 60% ductility by a reduction of austenite stability. *Acta Mater* 2011;59:4653–64. <https://doi.org/10.1016/j.actamat.2011.04.011>.
- [22] Mirshekari B, Zarei-Hanzaki A, Barabi A, Moshiri A, Abedi HR, Lee S-J, et al. Optimizing the austenite stability in a ferritic

- lightweight steel through thermomechanical processing. *Mater Char* 2020. <https://doi.org/10.1016/j.matchar.2020.110367>.
- [23] Mirshekari B, Zarei-hanzaki A, Barabi A, Abedi HR, Lee SJ, Fujii H. Materials Science & Engineering A an anomalous effect of grain refinement on yield stress in friction stir processed lightweight steel. *Mater Sci Eng, A* 2021;799:140057. <https://doi.org/10.1016/j.msea.2020.140057>.
- [24] Lee SJ, Park TM, Nam JH, Choi WS, Sun Y, Fujii H, et al. The unexpected stress-strain response of medium Mn steel after friction stir welding. *Mater Sci Eng, A* 2019;744:340–8. <https://doi.org/10.1016/j.msea.2018.12.041>.
- [25] Kim MT, Park TM, Baik KH, Choi WS, Han J. Effects of cold rolling reduction ratio on microstructures and tensile properties of intercritically annealed medium-Mn steels. *Mater Sci Eng, A* 2019;752:43–54. <https://doi.org/10.1016/j.msea.2019.02.091>.
- [26] Koyama M, Tasan CC, Akiyama E, Tsuzaki K, Raabe D. Hydrogen-assisted decohesion and localized plasticity in dual-phase steel. *Acta Mater* 2014;70:174–87. <https://doi.org/10.1016/j.actamat.2014.01.048>.
- [27] Selvam K, Prakash A, Grewal HS, Arora HS. Structural refinement in austenitic stainless steel by submerged friction stir processing. *Mater Chem Phys* 2017;197:200–7. <https://doi.org/10.1016/j.matchemphys.2017.05.034>.
- [28] Yan FK, Tao NR, Archie F, Gutierrez-Urrutia I, Raabe D, Lu K. Deformation mechanisms in an austenitic single-phase duplex microstructured steel with nanotwinned grains. *Acta Mater* 2014;81:487–500. <https://doi.org/10.1016/j.actamat.2014.08.054>.
- [29] Raposo M, Martín M, Giordana MF, Fuster V, Malarría J. Effects of strain rate on the TRIP–TWIP transition of an austenitic Fe-18Mn-2Si-2Al steel. *Metall Mater Trans A Phys Metall Mater Sci* 2019;50:4058–66. <https://doi.org/10.1007/s11661-019-05331-9>.
- [30] De Knijf D, Föjer C, Kestens LAI, Petrov R. Factors influencing the austenite stability during tensile testing of Quenching and Partitioning steel determined via in-situ Electron Backscatter Diffraction. *Mater Sci Eng, A* 2015;638:219–27. <https://doi.org/10.1016/j.msea.2015.04.075>.